High pressure ices

Andreas Hermann[a], N. W. Ashcroft[b,1], and Roald Hoffmann[a,1]

[a]Department of Chemistry and Chemical Biology, Cornell University, Ithaca, NY 14853; and [b]Laboratory of Atomic and Solid State Physics, Cornell University, Ithaca, NY 14853

Contributed by Roald Hoffmann, November 16, 2011 (sent for review September 9, 2011)

H_2O will be more resistant to metallization than previously thought. From computational evolutionary structure searches, we find a sequence of new stable and meta-stable structures for the ground state of ice in the 1–5 TPa (10 to 50 Mbar) regime, in the static approximation. The previously proposed *Pbcm* structure is superseded by a *Pmc*2_1 phase at $p = 930$ GPa, followed by a predicted transition to a *P*2_1 crystal structure at $p = 1.3$ TPa. This phase, featuring higher coordination at O and H, is stable over a wide pressure range, reaching 4.8 TPa. We analyze carefully the geometrical changes in the calculated structures, especially the buckling at the H in O-H-O motifs. All structures are insulating—chemistry burns a deep and (with pressure increase) lasting hole in the density of states near the highest occupied electronic levels of what might be component metallic lattices. Metallization of ice in our calculations occurs only near 4.8 TPa, where the metallic *C*2/*m* phase becomes most stable. In this regime, zero-point energies much larger than typical enthalpy differences suggest possible melting of the H sublattice, or even the entire crystal.

hydrogen bonds | compressed water

The phase diagram of H_2O exhibits a substantial array of stable and meta-stable crystalline phases, along with two amorphous ices (1). Terrestrial experiment continues to find new phases (2). There are also good cosmochemical reasons to think about the high pressure phases of H_2O—ice is a major component of the outer planets in our solar system, presumably forming very dense layers around the rocky cores of Neptune and Uranus (3, 4). And it is likely that ice will be a constituent of similarly sized or larger exoplanets that are currently being discovered (5, 6).

Known and Postulated Ice Structures

As ice is compressed at low temperatures from its hexagonal phase Ih at $P = 1$ atm, it undergoes a series of phase transitions between different molecular structures. At about 120 GPa, ice is expected to reach a hydrogen-ordered phase, ice X (7–10), in which individual molecules of H_2O are no longer discernible. Instead, the hydrogen atoms are located midway between nearest neighbor oxygen atoms, which in turn occupy body centered cubic lattice sites. The O-H distances in ice X are longer than intramolecular O-H distances in an isolated water molecule, or in ice Ih.

At even higher pressures, ice X is found from molecular dynamics simulations to give way to a *Pbcm* structure (11) between 300 and 400 GPa. Recently, calculations on symmetric structures where hydrogen occupies midpoints between nearest and next nearest neighbor oxygen atoms found phase transitions from *Pbcm* to a *Pbca* and a *Cmcm* structure at 760 and 1,550 GPa, respectively (12). The latter was also calculated to be metallic. Here, we present several new phases of ice calculated to be stable at pressures above 1 TPa. We find the most stable phases to be insulating, hence pushing the transition pressure for metallization of ice beyond 4.8 TPa (corresponding to ∼12-fold compression).

Searching Methodology

Finding thermodynamically stable structures for solids of given stoichiometry is a notoriously difficult task (13), which remains true even for transitions between ground state structures, as considered in what follows. When chemical intuition (14) fails one possible method to effectively and efficiently sample the configurational space of solid state structures for a given stoichiometry utilizes genetic or evolutionary algorithms. Such algorithms have been used originally for isolated molecules and clusters, (15–17), but also for extended systems (18, 19). Genetic or evolutionary algorithms rely on concepts borrowed from biological evolution to locate the global minimum on the potential energy surface. Here, we use the open source program *XtalOpt* (20) to perform an evolutionary algorithm based structure search. For a proposed structure the enthalpies are computed by density functional theory (DFT) with the *VASP* software package (21), making use of the Perdew-Burke-Ernzerhof parametrization of the exchange-correlation energy density (22), and the Projector Augmented Wave (PAW) method to describe the electron-ion interaction (23, 24). We use "hard" PAW datasets, with outermost cutoff radii for hydrogen and oxygen of 0.8 and 1.1 Bohr radii, respectively. A plane wave energy cutoff of 800 eV was employed, and Brillouin zones were sampled with a linear k-point density of 20 Å.

We performed structure searches at $p = 1$ TPa and $p = 2$ TPa with $Z = 4$ molecules per unit cell, and used the above mentioned ice X, *Pbcm*, and *Cmcm* structures, as well as random structures, as starting points for the workings of the evolutionary algorithm. As a check, a structure search at $p = 2.5$ TPa with $Z = 8$ molecules (unit cell doubled), and a structure search at $p = 5.0$ TPa with $Z = 4$ molecules, both seeded with all previously found low-enthalpy structures, did not result in new structures.

New Ices at Higher Pressures: Enthalpies

We find several new crystal structures of ice; these substantially change the phase diagram that theory has hitherto provided for the ground states at pressures above $p = 1$ TPa. Fig. 1 gives the computed enthalpies per H_2O at various pressures up to 2.5 TPa. A *Pmc*2_1 structure with four molecules per unit cell is enthalpically favored over the previously proposed *Pbca* structure above $p = 930$ GPa, and is succeeded above $p = 1{,}300$ GPa by a *P*2_1 structure, also with four molecules per unit cell. Remarkably, the relative stability of *P*2_1 ice increases rapidly over that of all previously known structures.

In addition to these most stable structures, we found a variety of other structures at $p = 2$ TPa, all more stable than any previously proposed structure. The enthalpies of the most competitive new structures are also shown in Fig. 1. Structural details of the new phases are listed in *SI Appendix*, Table SM1; the corresponding equation of state *V(p)* is given in *SI Appendix*, Fig. S1.

Structural Hallmarks of the Ice Structures Around 1 TPa

We begin with the *Pmc*2_1 structure, which is in our calculations the most stable phase (not by much, and more on this later) in the range $p = 1$ to 1.3 TPa. The *Pmc*2_1 structure, shown in the right column of Fig. 2, in contrast to the *Pbcm* structure, ice X, and other ice phases at lower pressures, does not feature two inter-

Author contributions: A.H., N.W.A., and R.H. designed research; A.H. and R.H. performed research; A.H. contributed new reagents/analytic tools; A.H., N.W.A., and R.H. analyzed data; and A.H., N.W.A., and R.H. wrote the paper.

The authors declare no conflict of interest.

[1]To whom correspondence may be addressed. E-mail: rh34@cornell.edu or nwa@ccmr.cornell.edu.

This article contains supporting information online at www.pnas.org/lookup/suppl/doi:10.1073/pnas.1118694109/-/DCSupplemental.

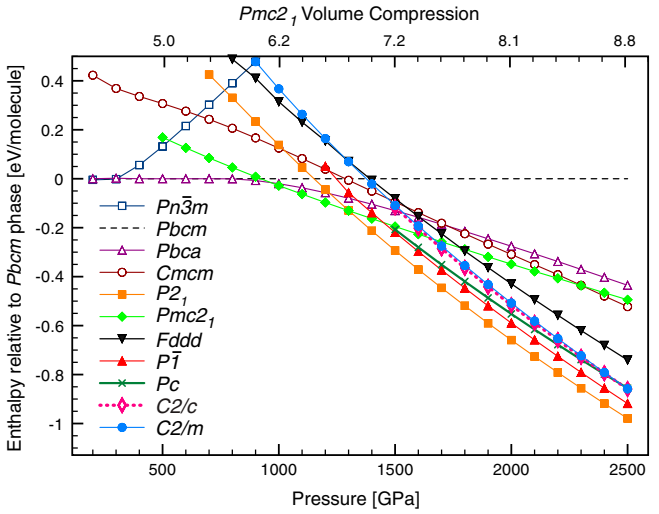

Fig. 1. Relative ground state enthalpies of known and new ice crystal phases. Zero-point motion is not included. Upper horizontal axis shows the volume compression of $Pmc2_1$ phase relative to ice XI (the H-ordered ground-state phase of ice) at $P = 1$ atm (25).

penetrating fourfold coordinated hydrogen bonded networks. Instead, the entire crystal is connected by pairwise O-H-O bridging bonds.

Putting the $Pmc2_1$ structure in a sequence with the ice X and *Pbcm* structures, a picture emerges (see Fig. 2) that illuminates the transition with increasing pressure from three-dimensional interpenetrating networks to two-dimensional corrugated sheets (12). In the transition from ice X to *Pbcm* the topology of O-H-O bridging bonds remains the same but adjacent layers in the *ab* plane are sheared with respect to each other, while all bridging bonds remain linear. In the transition from *Pbcm* to $Pmc2_1$, O-H-O bonds in half of these layers rearrange to form O-H-O bonds in a different direction (roughly they change from along the *b* axis to along the *a* axis), hence connecting previously independent networks. These bonds are buckled (the O-H-O angle is $\theta = 146°$ at $p = 1.2$ TPa), and the O atoms that are involved in the buckled bonds deviate significantly from ideal tetrahedral coordination.

Fig. 2, *SI Appendix*, Fig. S2 illustrate this structural sequence and the role of the $Pmc2_1$ structure as a successor of the $Pn\bar{3}m$ and *Pbcm* structures—and also as a precursor to the *Cmcm* structure, into which it would transform at about $p = 2.3$ TPa, were it not for a slew of other, more stable structures, which are discussed below. We find that a direct interpolation transition path between the *Pbcm* and the $Pmc2_1$ structure at $p = 700$ GPa has to overcome a transition barrier of only 0.11 eV per molecule (which may be compared with a zero-point energy of 1.00 eV per molecule, see below).

Structures Above 1 TPa

At $p = 1.3$ TPa the $P2_1$ structure becomes the most stable structure, and remains such up to 4.8 TPa. The $P2_1$ structure, see Fig. 3, is a three-dimensional O-H-O bonded network. It is the first

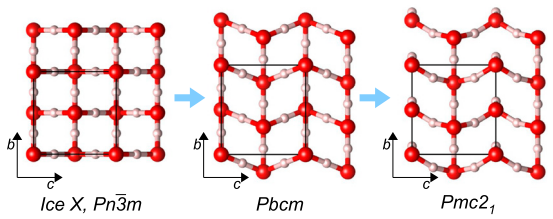

Fig. 2. From left to right: crystal structures of ice X ($Pn\bar{3}m$), *Pbcm*, and $Pmc2_1$, seen along the *a* axis. Unit cells are indicated ($\sqrt{2} \times \sqrt{2}$ cell for ice X). All structures are at $p = 700$ GPa (and ground-states).

stable ice structure where O atoms are clearly more than fourfold coordinated to H atoms; that in turn implies that H atoms are more than twofold coordinated to neighboring O atoms.

If a coordination number is defined via a "largest gap" definition in the neighbor distance histograms, then all O atoms in the $P2_1$ structure are fivefold coordinated to H atoms, and thus half of the H atoms in the crystal are threefold coordinated to neighboring O atoms (see *SI Appendix*, Fig. S3 for the histogram plots). The O-H connections drawn in Fig. 3 correspond to this definition of coordination.

The $P2_1$ structure recites structural elements seen in lower pressure structures: half of its O atoms form linear chains along the *b* axis (kinked along *c*), see the middle box of Fig. 3. These chains have almost linear O-H-O bonds ($\theta = 171°$ at $p = 2$ TPa), and are the basic building block of e.g., the *Cmcm* structure, cf. *SI Appendix*, Fig. S2. The remaining O atoms form a highly distorted bonded network, see middle box of Fig. 3 (but even there an imaginative eye might discover kinked chains along the *b* axis, connected through buckled and twisted O-H-O bonds).

In the right box of Fig. 3, we show both "sublattices" together: the quasi-linear and the severely twisted chains alternate along the *a* axis. These two sublattices are of course connected, and separating them as we do is to some extent arbitrary. However, this specific decomposition of the structure shows what drives its stabilization: it seems that kinked linear O-H-O-connected chains are a desired feature for ice under pressure, as they occur in the *Pbcm*, the $Pmc2_1$, and also the *Cmcm* structures. Beyond $p = 1.3$ TPa, however, it is preferred if some of these chains "give in" and form buckled, hence more compact, networks. The persistence of the linear chain motif in a sublattice of the $P2_1$ structure is a remnant of its lower pressure alternatives. We will return later to the reasons the high pressure ice phases favor buckled O-H-O units.

Closely related to the $P2_1$ structure is a $P\bar{1}$ structure we find to be the second most stable crystal structure over a wide pressure range, see Fig. 1. The structure of the $P\bar{1}$ phase is shown in Fig. 4. Very similar to $P2_1$, the $P\bar{1}$ phase is also a three-dimensional O-H-O bonded network which, depending on the definition of the O coordination number, consists of two interpenetrating sublattices (as shown in Fig. 4) or a fully connected network. Again we can identify two sublattices of slightly kinked chains running along the *b* axis, see middle box of Fig. 4. Here, in contrast to the $P2_1$ structure where one chain is quasi-linear and the other one highly distorted, both chains are moderately buckled. Each O atom is connected to two neighboring chains, in a way that forms two separate networks. One of these is shown in the right box of Fig. 4: instead of buckled chains with O-H-O connections, it can also be seen as sheets of edge-sharing $(OH)_6$ rings connected by O-H-O motifs. Either way, the $P\bar{1}$ structure shows us a different structural path away from linearly O-H-O connected chains. Ultimately, we find that at $p = 4.2$ TPa (static calculation) the $P\bar{1}$ structure becomes unstable with respect to the $C2/m$ structure.

Several other new structures, of *Pc*, $C2/c$, and *Fddd* symmetry, were found to be within 0.2 eV/molecule of the most stable $P2_1$ structure. The structural details of these phases are given in the *SI Appendix*.

Phase Transitions Near 5 TPa

Boldly extending the enthalpy curves of the most favored $P2_1$ and $C2/m$ structures to even higher pressures, we find a transition from the $P2_1$ to the $C2/m$ phase at $p = 4.8$ TPa. The evolution in enthalpy of various phases to high pressures is shown in Fig. 5 (note the relative enthalpies in Fig. 5 are now referred to those of the $P2_1$ phase).

The $C2/m$ structure is closely related to the *Cmcm* phase, see Fig. 6; whereas the latter comprises stacked corrugated sheets internally connected through O-H-O bridging bonds buckled *inwards*, the former features pairwise interpenetrating corrugated

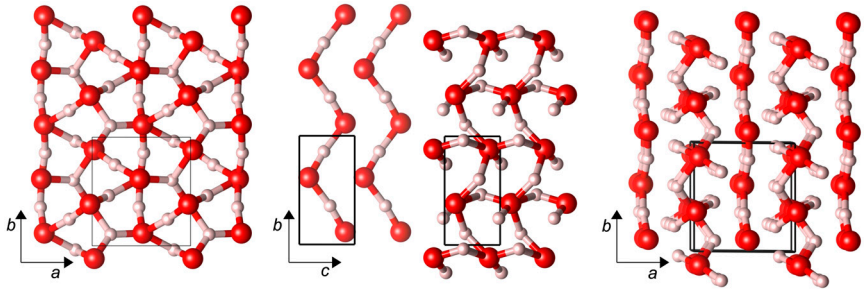

Fig. 3. Various views of the $P2_1$ structure. Left: along *c* axis; middle: two sublattices (see text), along *a* axis; right: superposition of sublattices, view close to *c* axis.

sheets of the same topology, but internally connected through O-H-O bridging bonds these being buckled *outwards*. One consequence is that the $C2/m$ structure contains linear chains of H atoms spaced by $b/2$ along the *b* axis, with H-H distances ranging from 1.01 Å at $p = 1$ TPa to 0.92 Å at $p = 2.5$ TPa and 0.88 Å at $p = 4$ TPa.

Such short H-H separations happen to be in the range of H-H separations in elemental hydrogen under pressure, at least as the latter is approximated in calculation. In the recent McMahon and Ceperley work on hydrogen in roughly the same pressure range that we cover, H-H separations between 0.87 Å ($p = 1.5$ TPa) and 0.83 Å ($p = 5.0$ TPa) are obtained for various structures of atomic hydrogen (26).

Another view of the $C2/m$ structure is that it is inherently two-dimensional, featuring bilayers of interpenetrating sheets in the *ab* plane which are not connected along the *c* axis. However, as we will see, structural low-dimensionality is not reflected on the electronic level—and this holds true also for the *Cmcm* structure. We do find that both the $C2/m$ and *Cmcm* structures, at very high pressures (from about $p = 4$ TPa onwards), exhibit an interesting fivefold O atom coordination, similar to the $P2_1$ structure discussed above: this happens as adjacent corrugated sheets are pressed closer to each other along the *c* axis (*b* axis for *Cmcm*), and intersheet O-H distances decrease to approach intrasheet O-H distances.

Dynamical Properties

To examine possible changes arising from departures from the static lattice approximation we studied the dynamical stability of these new structures using the PHON program (27), calculating the emerging force constant matrices within the harmonic approximation (see *SI Appendix* for more detailed information). The enthalpically stable phases are also dynamically stable in their respective pressure ranges: $Pmc2_1$ for $p = 1 \ldots 1.3$ TPa, and $P2_1$ for $p \geq 1.3$ TPa. Other structures are meta-stable. The zero-point vibrational energies (ZPE) for all phases are large, ranging (for the $P2_1$ structure) from 1.06 eV/molecule at $p = 1$ TPa via 1.37 eV/molecule at $p = 2.5$ TPa to 1.70 eV/molecule at $p = 5$ TPa. As might be expected, most of this zero-point energy resides in motion of the hydrogens (e.g., 1.06 eV/molecule at $p = 2.5$ TPa). However, differences in ZPEs among the various phases are below 50 meV/molecule, and thus are smaller than characteristic total energy differences between the phases for pressures $p \leq 2.5$ TPa. The inclusion of the ZPEs, however, shifts the transition pressure for the $Pbcm \rightarrow Pmc2_1$ transition to 880 GPa, and for the $Pmc2_1 \rightarrow P2_1$ transition to 1,170 GPa.

For pressures larger than $p = 2.5$ TPa, several phases come very close to each other in enthalpy, and inclusion of their ZPEs actually changes their enthalpic order. The $P\bar{1}$ structure becomes the most stable phase at $p = 3.6$ TPa, and its transition into the $C2/m$ phase does not happen until about $p = 6$ TPa. *SI Appendix*, Fig. S4 shows the evolution of the enthalpy curves of these phases with zero-point effects included. Even though the latter differ by only 2.5% (comparing e.g., the $P\bar{1}$ and $P2_1$ phases at $p = 3.6$ TPa), this is sufficient to overcome the total energy difference between these phases, and substantially shift the transition pressures and thus also the onset of stability of metallic ice.

The phonon dispersion relations and density of states for the $P2_1$ structure at $p = 2$ TPa are shown in *SI Appendix*, Fig. S5. Vibrations of the H sublattice reach frequencies of 150 THz, or 5,000 cm^{-1} (or over 500 meV). Such frequencies are quite high, but they are reasonable, as a molecular model we study below will show.

Metallic Ice?

Previous static calculations have suggested a transition to a metallic ice phase at pressure less than $p = 2$ TPa. We find more stable phases in this pressure regime, and they are far from metallic even though the bands are quite wide (about 50–55 eV). The $Pmc2_1$, $P2_1$, and $P\bar{1}$ structures are calculated to be insulating, with substantial band gaps of more than 3 eV even at $p = 2.5$ TPa, see Fig. 7. The trend of large band gaps in molecular and atomic ice phases, which even *increase* initially under pressure (25), is continued. The only metallic structure we find, $C2/m$, whose DFT band gap in our calculations closes at $p = 1.1$ TPa, is just not competitive in this pressure regime, see Fig. 1.

Fig. 7 (top box) illustrates both the traditional notion that insulating phases, where such may exist, are favored over coexisting

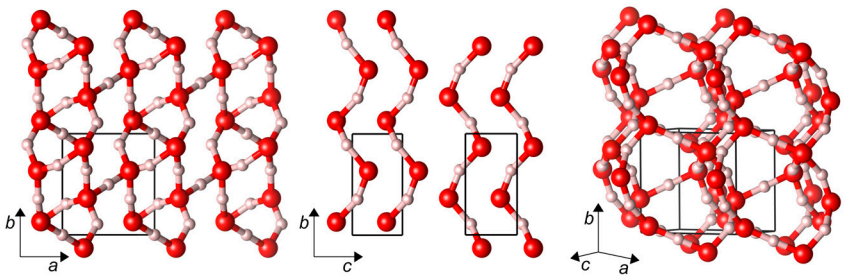

Fig. 4. Various static lattice views of the $P\bar{1}$ structure. Left: along the *c* axis; middle: the two sublattices, along the *a* axis; right: one of the two interpenetrating networks.

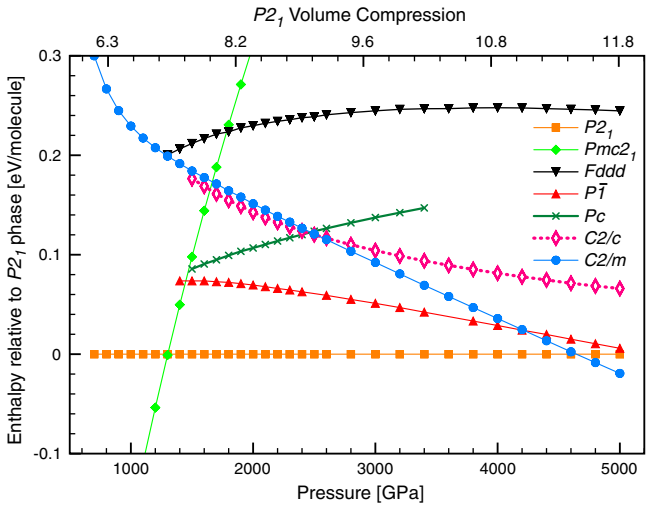

Fig. 5. Ground state enthalpies of new ice structures up to $p = 5$ TPa, relative to the $P2_1$ structure. Upper x axis gives the volume compression of $P2_1$ structure relative to ice XI at 1 atm.

metallic phases. And that there is no correlation between stability and size of the band gap for these insulating phases.

However, at the top of the pressure range we study statically, at $p = 4.8$ TPa, a metallic phase, $C2/m$, does become more stable than its insulating competitors (dynamical effects shift this onset of metallization to even higher pressures). The electronic density of states (DOS) for this phase is also shown in Fig. 7 (bottom box), its band structure is plotted in *SI Appendix*, Fig. S6. The valence bandwidth at almost 5 TPa pressure is about 60 eV; the DOS is very much free-electron like at low energies, with minor features that correspond to the pseudopotential. At the Fermi level, however, the DOS is depleted significantly (for free electrons it would be $3/2E_f$ or 0.025 states per electron per eV), making the $C2/m$ phase a rather ordinary metal even at these high pressures. There is no sign, however, of low-dimensional electronic character, and neither can it be found in the *Cmcm* structure (see *SI Appendix*, Fig. S7 for its electronic DOS).

Chemistry

While $P2_1$ is insulating, at its stability onset of $p = 1.3$ TPa both its O and H sublattices would separately be metallic. There are two ways to think about the insulating character of ice: One is to say that OH bond formation, partially covalent, burns a deep gap in the DOS at the Fermi level. Alternatively, coexistence of O and H in the lattice allows the electron transfer that electronegativity

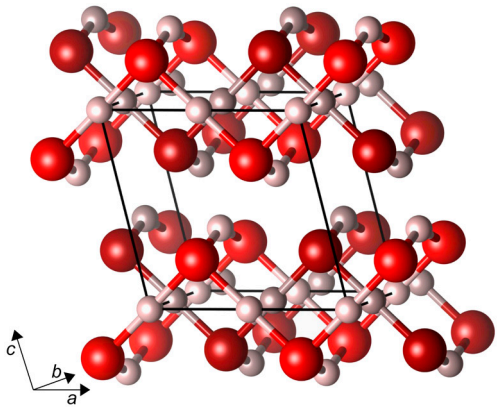

Fig. 6. Static crystal structure of $C2/m$ phase, at $p = 2$ TPa. Different levels of brightness of atoms indicate separate sublattices.

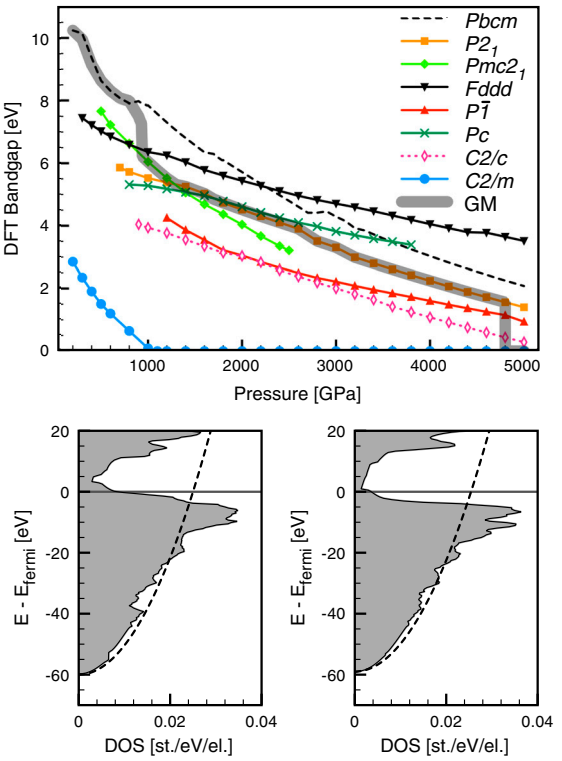

Fig. 7. Top: DFT band gaps for various static ice structures, up to $p = 5$ TPa; the gray band indicates the global minimum (GM) band gap curve. Bottom: electronic DOS (in states per electron per eV) for metallic $C2/m$ phase and its O^{2-} sublattice, at $p = 4.8$ TPa. The dashed line in the DOS plots indicates a free-electron DOS per electron with a bandwidth of 60 eV (left) and 59 eV (right).

mandates, this towards a formal $(H^+)_2(O^{2-})$ extreme. And the configuration of these ions is a closed shell one. Either way, chemistry makes a tremendous difference.

Even when metallicity appears around 5 TPa, the ionic perspective retains its value. Consider the band structure and DOS of the O^{2-} sublattice of the $C2/m$ structure at 4.8 TPa—a calculation on a lattice of O^{2-} ions at the same positions as the oxygens in $C2/m$, with the H atoms removed and replaced by a constant background charge compensating the excess electronic charge of the unit cell—as shown in the bottom box of Fig. 7 and in *SI Appendix*, Fig. S6. The two electronic structures—H_2O and the O^{2-} sublattice—are very similar. Highly compressed ice therefore behaves like a network of highly compressed oxide ions—the presence of the protons is necessary to avoid a Coulomb explosion, but nevertheless changes the electronic properties very little. The same is true for the insulating $P2_1$ phase (see *SI Appendix*, Fig. S8). O^{2-} is isoelectronic to neon; perhaps this makes it less surprising to see ice remain insulating to very high pressure.

Is Water More or Less Polar When Pressurized?

Water in its extended phases has an increased dipole moment compared to the single molecule (28, 29) (although it may be prudent to have some reservations about identifying electrostatic moments in the close quarters of a molecular crystal, especially under high pressures). In the structures beyond ice X we study, there are no identifiable water molecules. But we can still think about the ionicity of the O and H components. There is an inherent difficulty in assigning electronic density to individual atoms when using plane wave basis sets. Here, we choose to project the valence charge density onto atomic spheres around each atom that just touch; i.e., the O and H sphere radii r_O and r_H are adjusted to add up to the shortest O-H distance at each pressure, with $r_O = 2 \times r_H$ (roughly the cube roots of the atom/ion valence

electron counts). Then, we scale these localized electron counts such that they add up to the number of electrons in the unit cell. If we compare the electron densities/charges thus obtained (see *SI Appendix*, Fig. S9), we find a slight decrease in ionicity under pressure, and for all competitive high pressure phases. To be specific, the valence electron density on O (which should be six electrons for a neutral atom) reduces from 7.22 at 2 TPa to 7.12 at 4.8 Tpa.

We also tried to assign charges to atoms through a topological analysis of the electronic density (30, 31). We obtain similar electron densities to those found with the method described above—with a still less pronounced trend under increased pressure, and with highly distorted atom-centered domains around the O atoms.

We might mention at this point a general concern about electron density in highly compressed matter, and this pertains to valence electron density as we move away from the nuclei. Such deformations were first found for elemental lithium (32) and have since been observed for other elemental structures. We looked carefully for this phenomenon in ice, and found even at the highest pressures no density maximum in the interstitial space between the atoms.

Why do Hydrogens go "Nonlinear" at High Pressures?

The progression we see in H_2O structures as the pressure rises has some expected features, and also some unusual ones. The expected feature is a rise in coordination at O and at H, starting from the molecular two-coordination at the oxygen and singly coordinated hydrogens. In the ice X structure we find four-coordination (in H) at O, and two-coordination at H. And, as we have seen, higher pressure brings us to still higher coordination at O and at H.

An interesting geometrical feature we find in the structures evolving after ice X is that the O-H-O linkage goes progressively nonlinear at H. Why does this nonlinearity happen? We investigated this effect with a molecular model, shown in Fig. 8. Two water molecules were brought together in a classical hydrogen bonding arrangement except that the O-H-O central unit was kept symmetrical (both OH separations maintained as equal) and linear. The OO separation (a surrogate for pressure) was then varied, and the normal modes of vibration for the central H atom then calculated [here using the Gaussian program suite, the B3LYP exchange-correlation functional, and augmented triple zeta basis sets (33–36)].

In Fig. 8, the normal mode (vibron) at around 1,400 cm^{-1} is the OHO-bending vibration, and the rising higher frequency mode is the asymmetric stretch. If we let the central hydrogen depart from left-right equality, or OHO colinearity, it indeed would do so outside the region 2.52 Å ≥ r(OO) ≥ 2.03 Å. At longer O-O separations the hydrogen would remain linear (or at least close to linear), but move closer to one oxygen, at shorter O-O it would go out-of-the-line, or buckle. In the calculated ice phases, the stability onset of symmetrically bonded ice X is at $p = 120$ GPa, with $r_{OO} = 2.27$ Å; and the first buckled O-H-O bonds in ice occur at $p = 800$ GPa in the *Pbca* structure, where $r_{OO} = 1.97$ Å. Observe how nicely the appearance of imaginary frequencies in the simple molecular model now agrees with these onsets of departure from symmetric linear geometry for O-H-O. An even simpler ansatz, suggested to us by a reviewer, where both the O-H and the O-O interaction are described by Morse potentials (37), leads qualitatively to the same result (see the *SI Appendix* for more details).

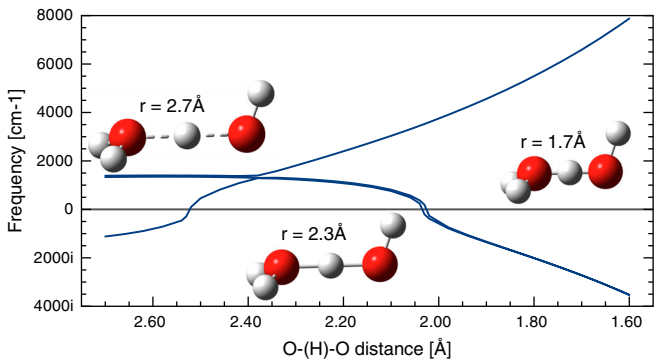

Fig. 8. Vibrational frequencies for H atom in the center-position of the O-H-O bridging bond (see text).

But the question still remains: why do the hydrogens go offline? We think the answer is that under pressure one needs to increase further the O coordination in other *oxygens* and not only *hydrogens*. And that is most simply accomplished by bending at the hydrogens.

High Zero-Point Energies and a Possible Liquid Phase

As we see in the molecular model discussed above, the vibration of H along the O-H-O axis indeed reaches the substantial value of 5,000 cm^{-1} and more (exceeding 0.6 eV), if the oxygen atoms are brought to within $r_{OO} = 1.80$ Å or less. This energy is at the top of the frequency spectrum for the $P2_1$ phase at $p = 2$ TPa, see *SI Appendix*, Fig. S5. Accordingly might the high zero-point vibrational energies associated with this H motion then perhaps result in a melting of the H sublattice, or even the whole ice crystal structure at sufficiently high pressures? The phenomenon of reentrant melting under pressure has been found recently, for example, in the alkali metals Li and Na (38–40), and the dissociation of *hot* dense water and different mobilities for its constituents H and O have been reported both from molecular dynamics simulations and experiment (41–43).

In support of the notion of *cold* superionic high pressure ice it may be mentioned that a typical barrier to concerted diffusion of H atoms between lattice sites in the $P2_1$ structure at $p = 2$ TPa is just 0.7 eV, (to be compared with 0.5 eV as the hydrogen and harmonic approximation based zero-point energy). There are certainly a variety of crystalline phases with very similar enthalpies of formation at $p \geq 4$ TPa, and the zero-point energies are also much larger than their enthalpy differences. It is not hard to imagine that at least the protons would use the zero-point motion to adopt a fluctuating mixture of crystalline phases; i.e., a liquid and in this context the replacement of hydrogen by deuterium could be quite revealing. Either for water or for heavy water the issue of metallization possibly setting in earlier, in association with the diffusive or sublattice melted state, then becomes quite pertinent.

Conclusions

To summarize, we have found a number of new ground state phases of ice under extremely high pressures but perhaps typical of some planetary conditions. A revised phase diagram for ice in the TPa pressure regime is suggested, with a phase transition into a $Pmc2_1$ structure at $p = 0.93$ TPa followed by a transition into a $P2_1$ structure at $p = 1.3$ TPa. Both of these phases are large gap insulators. Clearly, the interaction of O and H makes a difference —chemistry "burns" a large and persistent (with pressure) hole in the upper reaches of the density of states of two metallic sublattices, O and H. Or, alternatively, the capacity for electron transfer from H to O, makes compressed H_2O very different from its neutral sublattices.

In the new high pressure ices that we propose, we see a tendency to buckle or bend at the H in O-H-O motifs, a phenomenon we trace to the increased coordination made available by this motion. Metallization of ice is not found until $p = 4.8$ TPa in static calculations (and even higher when dynamical effects are estimated at the level of the harmonic approximation), when a $C2/m$ structure, this related to a recently suggested *Cmcm* structure, becomes the most stable phase. These findings, especially

the "delayed" metallization of ice, should have significance beyond the ground states considered here and hence for modeling the interiors of some massive gas planets. There is another possibility that also merits further examination, namely that because of the possible onset of H (or D) diffusion, high pressure ices may adopt fluid states. After our work was completed, we became aware of several new studies of high pressure ice phases (44–46). The structures obtained in these studies mostly agree with ours.

ACKNOWLEDGMENTS. Andreas Hermann wishes to acknowledge Peter Schwerdtfeger for piquing his interest in high pressure studies of water and ice. We thank two reviewers for their comments. Our work was supported by EFree, an Energy Frontier Research Center funded by the Department of Energy (Award Number DESC0001057 at Cornell) and the National Science Foundation through Grants CHE-0910623 and DMR-0907425. Computational resources provided by the Cornell NanoScale Facility (supported by the National Science Foundation through Grant ECS-0335765), and by the TeraGrid network (provided by the National Center for Supercomputer Applications through Grant TG-DMR060055N), are gratefully acknowledged.

1. Petrenko VF, Whitworth RW (1999) *Physics of Ice* (Oxford University Press, Oxford).
2. Salzmann CG, Radaelli PG, Mayer E, Finney JL (2009) Ice XV: A New Thermodynamically Stable Phase of Ice. *Phys Rev Lett* 103:105701.
3. Ross M (1981) The ice layer in Uranus and Neptune—diamonds in the sky? *Nature* 292:435–436.
4. Podolak M, Weizman A, Marley M (1995) Comparative models of Uranus and Neptune. *Planet Space Sci* 43:1517–1522.
5. Beaulieu J-P, et al. (2006) Discovery of a cool planet of 5.5 Earth masses through gravitational microlensing. *Nature* 439:437–440.
6. Gould A, et al. (2006) Microlens OGLE-2005-BLG-169 implies that cool neptune-like planets are common. *Astrophys J* 644:L37–L40.
7. Benoit M, Marx D, Parrinello M (1998) Tunnelling and zero-point motion in high-pressure ice. *Nature* 392:258–261.
8. Loubeyre P, LeToullec R, Wolanin E, Hanfland M, Hausermann D (1999) Modulated phases and proton centring in ice observed by X-ray diffraction up to 170 GPa. *Nature* 397:503–506.
9. Benoit M, Romero AH, Marx D (2002) Reassigning hydrogen-bond centering in dense ice. *Phys Rev Lett* 89:145501.
10. Caracas R (2008) Dynamical instabilities of ice X. *Phys Rev Lett* 101:85502.
11. Benoit M, Bernasconi M, Focher P, Parrinello M (1996) New high-pressure phase of ice. *Phys Rev Lett* 76:2934–2936.
12. Militzer B, Wilson HF (2010) New phases of water ice predicted at megabar pressures. *Phys Rev Lett* 105:195701.
13. Maddox J (1988) Crystals from first principles. *Nature* 335:201 201.
14. Grochala W, Hoffmann R, Feng J, Ashcroft N (2007) The chemical imagination at work in very tight places. *Angew Chem Int Edit* 46:3620–3642.
15. Hartke B (1993) Global geometry optimization of clusters using genetic algorithms. *J Phys Chem* 97:9973–9976.
16. Johnston RL (2003) Evolving better nanoparticles: genetic algorithms for optimising cluster geometries. *Dalton T* 4193–4207.
17. Assadollahzadeh B, Bunker PR, Schwerdtfeger P (2008) The low lying isomers of the copper nonamer cluster, Cu9. *Chem Phys Lett* 451:262–269.
18. Oganov AR, Lyakhov AO, Valle M (2011) How evolutionary crystal structure prediction works-and why. *Acc Chem Res* 44:227–237.
19. Zurek E, Hoffmann R, Ashcroft NW, Oganov AR, Lyakhov AO (2009) A little bit of lithium does a lot for hydrogen. *Proc Natl Acad Sci USA* 106:17640–17643.
20. Lonie DC, Zurek E (2011) XtalOpt: An open-source evolutionary algorithm for crystal structure prediction. *Comput Phys Commun* 182:372–387.
21. Kresse G, Furthmüller J (1996) Efficient iterative schemes for {it ab initio} total-energy calculations using a plane-wave basis set. *Phys Rev B* 54:11169–11186.
22. Perdew JP, Burke K, Ernzerhof M (1996) Generalized gradient expansion made simple. *Phys Rev Lett* 77:3865–3868.
23. Blöchl PE (1994) Projector augmented-wave method. *Phys Rev B* 50:17953–17979.
24. Kresse G, Joubert D (1999) From ultrasoft pseudopotentials to the projector augmented-wave method. *Phys Rev B* 59:1758–1775.
25. Hermann A, Schwerdtfeger P (2011) Blueshifting the onset of optical UV absorption for water under pressure. *Phys Rev Lett* 106:1–4.
26. McMahon J, Ceperley D (2011) Ground-state structures of atomic metallic hydrogen. *Phys Rev Lett* 106:165302.
27. Alfè D (2009) PHON: A program to calculate phonons using the small displacement method. *Comput Phys Commun* 180:2622–2633.
28. Silvestrelli PL, Parrinello M (1999) Water molecule dipole in the gas and in the liquid phase. *Phys Rev Lett* 82:3308.
29. Batista ER, Xantheas SS, Jónsson H (1998) Molecular multipole moments of water molecules in ice Ih. *J Chem Phys* 109:4546–4551.
30. Bader RFW (1994) *Atoms in Molecules: A Quantum Theory* (Oxford University Press, New York).
31. Tang W, Sanville E, Henkelman G (2009) A grid-based Bader analysis algorithm without lattice bias. *J Phys-Cond Mat* 21:084204.
32. Neaton JB, Ashcroft NW (1999) Pairing in dense lithium. *Nature* 400:141–144.
33. Frisch MJ, et al. (2004) (Gaussian, Inc., Wallingford, CT) Gaussian 09 Revision A.02.
34. Becke AD (1993) A new mixing of Hartree-Fock and local density-functional theories. *J Chem Phys* 98:1372–1377.
35. Stephens PJ, Devlin FJ, Chabalowski CF, Frisch MJ (1994) Ab Initio calculation of vibrational absorption and circular dichroism spectra using density functional force fields. *J Phys Chem* 98:11623–11627.
36. Kendall RA, Dunning TH, Jr, Harrison RJ (1992) Electron affinities of the first-row atoms revisited. Systematic basis sets and wave functions. *J Chem Phys* 96:6796–6806.
37. Holzapfel WB (1972) On the symmetry of the hydrogen bonds in ice VII. *J Chem Phys* 56:712–715.
38. Gregoryanz E, Degtyareva O, Somayazulu M, Hemley R, Mao H-kwang (2005) Melting of dense sodium. *Phys Rev Lett* 94:1–4.
39. Guillaume CL, et al. (2011) Cold melting and solid structures of dense lithium. *Nat Phys* 7:211–214.
40. Rousseau B, Xie Y, Ma Y, Bergara A (2011) Exotic high pressure behavior of light alkali metals, lithium and sodium. *Eur Phys J B* 81:1–14.
41. Schwegler E, Galli G, Gygi F, Hood R (2001) Dissociation of water under pressure. *Phys Rev Lett* 87:265501.
42. Goldman N, Fried L, Kuo I-F, Mundy C (2005) Bonding in the superionic phase of water. *Phys Rev Lett* 94:217801.
43. Goncharov AF, et al. (2005) Dynamic ionization of water under extreme conditions. *Phys Rev Lett* 94:125508.
44. Wang Y, et al. (2011) High pressure partially ionic phase of water ice. *Nat Commun* 2:563–567.
45. McMahon J (2011) Ground-state structures of ice at high pressures from ab initio random structure searching. *Phys Rev B* 84:220104.
46. Ji M, et al. (2011) Ultrahigh-pressure phases of H_2O ice predicted using an adaptive genetic algorithm. *Phys Rev B* 84:220105.